SOILS AND FOUNDATIONS Vol. 47, No. 3, 507–516, June 2007
Japanese Geotechnical Society

THE INFLUENCE OF ANISOTROPIC STIFFNESS ON THE CONSOLIDATION OF PEAT

C. ZWANENBURG[i),ii)] and F. B. J. BARENDS[i),ii)]

ABSTRACT

An analytical solution for the consolidation problem of an axially loaded triaxial sample including anisotropy in stiffness is presented. The solution shows that anisotropy in stiffness strongly influences the consolidation process. The influence of anisotropy in stiffness is found in the initial pore pressure reaction, in the Mandel-Cryer effect and in the consolidation coefficient. Measurements on conventional sized peat samples appear not to correspond to the analytical solution. Besides drain resistance, literature presents two other explanations for this fact. These explanations are tested in a large scale test set-up. It is found that induced permeability changes have a strong influence. The possibility of using the Mandel-Cryer effect for assessment of stiffness parameters of peat introduces extra parameters to describe the variations in permeability. For strongly over-consolidated samples, leading to a nearly constant permeability the analytical solution fits perfectly to measurements.

Key words: anisotropy, elasticity, laboratory test, organic soil, pore pressure (**IGC**:D5)

INTRODUCTION

Consolidation of soft soil is one of the main problems of geomechanics. Many authors have studied consolidation problems or related problems. Still, not all phenomena and their interaction are fully understood. One of these phenomena deals with the redistribution of stresses. This paper studies this phenomenon including anisotropy in stiffness for a consolidating axial symmetric soil sample. In LITERATURE OVERVIEW, a short literature overview is presented. ANISOTROPIC SOIL BEHAVIOUR, PROBLEM DESCRIPTION and SOLUTION discuss the analytical solution for the axial-symmetric consolidation problem. MEASUREMENTS and LARGE SCALE TESTING discuss test results.

LITERATURE OVERVIEW

The pioneers who discussed the influence of a redistribution of stresses to the pore pressure development during consolidation are Mandel (1953) and Cryer (1963). Cryer considers a spherical soil sample which is drained at the outer radius. Due to an isotropic load increment the outer radius will consolidate almost instantaneously leading to volumetric strain in the outer skin of the sample. The outer skin compresses the inner core of the sample which still behaves undrained. Due to this compression the pore pressure increases in the inner core until consolidation reaches the inner part. Then monotonic pore pressure decay follows. Mandel (1953) shows equivalent results in a mathematical analysis. The phenomenon of initial pressure rise is referred to as the Mandel-Cryer effect. Gibson et al. (1964) show measurements of this phenomenon. De Leeuw (1964, 1965) and Kumamoto and Yoshikuni (1981) show the Mandel-Cryer effect for axial-symmetric conditions, based on the Biot solution for three-dimensional consolidation, *see* Biot (1941, 1955, 1957).

Al-Tabbaa and Wood (1991) and Al-Tabbaa (1992) discuss results of a numerical analysis and measurements for axial symmetric conditions including plastic material behaviour. Their analysis includes the influence of the strain condition at the top, free strain or uniform strain. Both conditions can be used to reproduce the Mandel-Cryer effect. However, for free vertical strain the numerical analysis predicts an initial decay in pore pressure preceding a reduced Mandel-Cryer peak in the middle of the sample.

Abousleiman et al. (1996) present an analytical solution for plane strain conditions including cross-anisotropic linear elastic material behaviour. The solution is illustrated by examples regarding soft rock. It is found that anisotropy strongly influences the Mandel-Cryer effect. Chen et al. (2005) give a semi-analytical solution to the axial-symmetric consolidation problem of a transversely isotropic soil layer subjected to a uniform circular load at ground surface.

This paper discusses the possibility of using measurements of pore pressure development inside soft soil samples, in particular peat, to derive information on the level of anisotropy in stiffness. Peat is an organic material which, depending on the rate of humification, can be

i) Delft University of Technology, The Nertherlands (c.zwanenburg@geodelft.nl).
ii) GeoDelft, The Netherlands.
The manuscript for this paper was received for review on January 10, 2006; approved on February 10, 2007.
Written discussions on this paper should be submitted before January 1, 2008 to the Japanese Geotechnical Society, 4-38-2, Sengoku, Bunkyo-ku, Tokyo 112-0011, Japan. Upon request the closing date may be extended one month.

considered as a fibrous material. Due to the strong heterogeneity anisotropic stiffness, parameters can hardly be obtained by testing different soil samples taken in different directions. If instead measurements of pore pressure development can be used to derive information on the level of anisotropy, an alternative assessment of material behaviour becomes available.

ANISOTROPIC SOIL BEHAVIOUR

Extending the De Leeuw solution to anisotropic linear elasticity requires an extension of Hooke's law. Assuming cross-anisotropic conditions with the axis of symmetry in vertical direction yields:

$$\varepsilon_{ij} = D_{ijkl}\sigma'_{kl} \tag{1}$$

with $D_{ijkl} =$

$$\begin{pmatrix} \frac{1}{E_h} & \frac{-\nu_{hh}}{E_h} & \frac{-\nu_{vh}}{E_v} & 0 & 0 & 0 \\ \frac{-\nu_{hh}}{E_h} & \frac{1}{E_h} & \frac{-\nu_{vh}}{E_v} & 0 & 0 & 0 \\ \frac{-\nu_{vh}}{E_v} & \frac{-\nu_{vh}}{E_v} & \frac{1}{E_v} & 0 & 0 & 0 \\ 0 & 0 & 0 & \frac{1}{G_{hh}} & 0 & 0 \\ 0 & 0 & 0 & 0 & \frac{1}{G_{vh}} & 0 \\ 0 & 0 & 0 & 0 & 0 & \frac{1}{G_{vh}} \end{pmatrix}$$

In which ε_{ij} represents the strain tensor, σ_{ij} the stress tensor, E_h the Young's modulus in horizontal direction, E_v the Young's modulus in vertical direction, ν_{vh} the Poisson's ratio for horizontal strain due to vertical strain, ν_{hh} the Poisson's ratio for horizontal strain due to horizontal strain, and G_{vh} the Shear modulus in vertical plane. As shown by Brodeau (1946) five is the minimum number of parameters to describe cross-anisotropy, since the shear modulus in the horizontal plane G_{hh} can be expressed in $G_{hh} = E_h/2(1+\nu_{hh})$.

Inversion of Eq. (1) gives:

$$\begin{aligned} \sigma'_{xx} &= Ae + 2G_{hh}\varepsilon_{xx} + B\varepsilon_{zz}, & \tau_{xy} &= G_{hh}\gamma_{xy} \\ \sigma'_{yy} &= Ae + 2G_{hh}\varepsilon_{yy} + B\varepsilon_{zz}, & \tau_{yz} &= G_{vh}\gamma_{yz} \\ \sigma'_{zz} &= (A+B)e + D\varepsilon_{zz}, & \tau_{zx} &= G_{vh}\gamma_{zx} \end{aligned} \tag{2}$$

with:

$$A = \frac{\nu_{hh}E_hE_v + \nu_{vh}^2E_h^2}{(1+\nu_{hh})(E_v(1-\nu_{hh}) - 2E_h\nu_{vh}^2)}$$

$$B = \frac{E_hE_v(\nu_{vh}(1+\nu_{hh}) - \nu_{hh}) - \nu_{vh}^2E_h^2}{(1+\nu_{hh})(E_v(1-\nu_{hh}) - 2E_h\nu_{vh}^2)}$$

$$D = \frac{E_v^2(1-\nu_{hh}) - E_hE_v\nu_{vh}}{E_v(1-\nu_{hh}) - 2E_h\nu_{vh}^2}$$

In which e represents the volumetric strain, τ the shear stress and γ the shear strain. Note that for isotropic conditions, $E_h = E_v = E$, $G_{hh} = G_{vh} = G$ and $\nu_{hh} = \nu_{vh} = \nu$, Eq. (2) reduces to $\sigma'_{ij} = \lambda e\delta_{ij} + 2\mu\varepsilon_{ij}$, in which λ and μ are the well-known Lamé constants, $\lambda = \nu E/[(1+\nu)(1-2\nu)]$ and $\mu = G$.

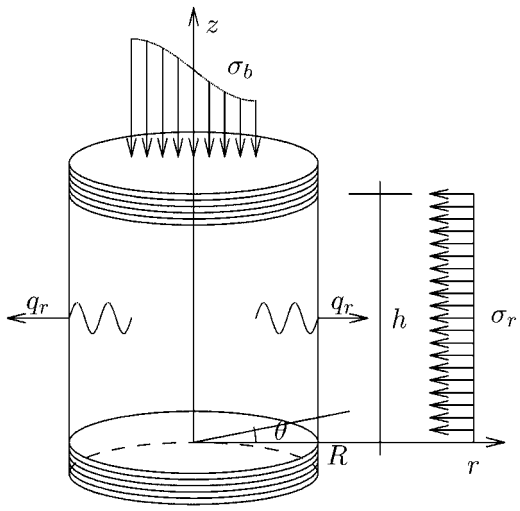

Fig. 1. Axial symmetric conditions

PROBLEM DESCRIPTION

Figure 1 sketches the problem, with σ_b the applied loading and q_r the expelled pore water flow. In solving this consolidation problem the following is assumed; uniform vertical strain leading to $\partial\varepsilon_z/\partial z = 0$ and $\partial\varepsilon_z/\partial r = 0$, axial-symmetry leading to all $\partial/\partial\theta = 0$, $\varepsilon_\theta = 0$ and $\tau_{zr} = \tau_{z\theta} = \tau_{\theta r} = 0$, the pore fluid is considered incompressible and pore water flow is described by Darcy's law. All stress and strain are chosen positive for tension; pore pressure is denoted by $-\sigma_w$.

The consolidation problem is solved for two different sets of boundary conditions, first for the case of an axially loaded triaxial sample and second for the isotropically loaded sample.

Conditions of equilibrium give in combination to Eq. (2) after some elaboration:

$$[A + 2G_{hh}]\nabla^2 e = \nabla^2\sigma_w \tag{3}$$

Since anisotropy in stiffness does not influence the storage equation, it remains unaltered. The storage equation, when neglecting the compressibility of the pore fluid, is given by Verruijt (1969):

$$\frac{k}{\gamma_w}\nabla^2\sigma_w = \frac{\partial e}{\partial t} \tag{4}$$

In which k represents the permeability, γ_w the volumetric weight of the pore fluid and t time. Eliminating σ_w gives the consolidation equation:

$$\nabla^2 e = \frac{1}{c}\frac{\partial e}{\partial t}, \quad c = [A + 2G_{hh}]\frac{k}{\gamma_w} \tag{5}$$

In which c is the consolidation coefficient for anisotropic conditions.

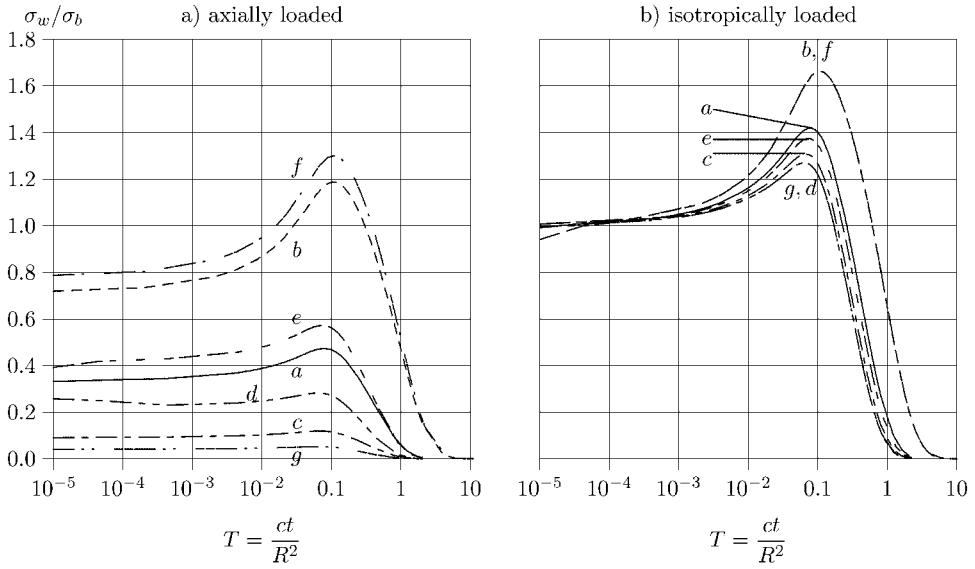

Fig. 2. Pore pressure development at $r/R = 0.02$ for axial-symmetric conditions *a* to *g* according to Table 1

SOLUTION

APPENDIX A discusses the analytical solutions for Eq. (5). A more detailed discussion on the analytical solution is given in Zwanenburg (2005). This paper focuses on the solution for the pore pressure development. For an axially loaded sample the following is found:

$$\frac{\sigma_w}{\sigma_b} = \sum_{j=1}^{\infty} \frac{\left[1 - \frac{J_0(\lambda_j r)}{J_0(\lambda_j R)}\right] \exp(s_j t)}{\alpha + \beta} \tag{6}$$

with:

$$\alpha = \frac{B - 2G_{hh} + DG_{hh}/(B - G_{hh})}{A + 2G_{hh}}$$

$$\beta = \left[\frac{\lambda_j R}{2} \frac{J_1(\lambda_j R)}{J_0(\lambda_j R)} - 1\right]\left[\frac{D}{B - G_{hh}} - 1\right]$$

For an isotropically loaded sample:

$$\frac{\sigma_w}{\sigma_b} = \sum_{j=1}^{\infty} \frac{\frac{B - G_{hh} - D}{B - G_{hh}}\left[1 - \frac{J_0(\lambda_j r)}{J_0(\lambda_j R)}\right] \exp(s_j t)}{\alpha + \beta} \tag{7}$$

With J_0 and J_1 representing Bessel functions, r the co-ordinate in radial direction, σ_b the applied load and $\lambda_j = \sqrt{-s_j/c}$ in which s_j represents the characteristics of the Laplace inverse transformation, in which s_j are the roots of:

$$\frac{J_1(\lambda R)}{J_0(\lambda R)} = \frac{1}{2}\left[\frac{A + 2G_{hh}}{B - 2G_{hh} + \frac{DG_{hh}}{B - G_{hh}}}\right]\left[\frac{D}{B - G_{hh}} - 1\right]\lambda R$$

Figure 2 visualises Eqs. (6) and (7) for seven different combinations of stiffness parameters, explained in Table 1 and $k = 1 \times 10^{-8}$ m/s. The solution, especially for case *d*, converges slowly for small values for r and t.

Figure 2 shows the influence of anisotropy in stiffness to the pore pressure development during consolidation.

Table 1. Seven cases for visualisation of solution (6) and (7), K'/J' defined by Eq. (8)

Case	E_h [kN/m²]	E_v [kN/m²]	ν_{hh} [—]	ν_{vh} [—]	c [10^{-6} m²/s]	K'/J' [—]
a (isotropic)	1000	1000	0	0	1.02	0
b	5000	1000	0	0	5.10	0.38
c	1000	5000	0	0	1.02	−0.24
d	1000	1000	0	0.3	1.13	−0.11
e	1000	1000	0.3	0	1.12	0.08
f	5000	1000	0.3	0	5.60	0.45
g	1000	5000	0	0.3	1.04	−0.29

The influence is most distinct for the axially loaded sample, Fig. 2(a). The size of the Mandel-Cryer peak is influenced by the anisotropy as well as the initial pore pressure reaction. This phenomenon is explained by the fact that undrained soil behaviour can be considered as constant volume deformation. For isotropic materials, volumetric strain is only initiated by an isotropic stress increment. Anisotropic materials, however, also show volumetric strain due to a deviatoric stress increment. Atkinson et al. (1990) present the following stress-strain relationship:

$$\begin{bmatrix} \delta e \\ \delta \varepsilon_q \end{bmatrix} = \begin{bmatrix} \frac{1}{K'} & \frac{1}{J'} \\ \frac{1}{J'} & \frac{1}{3G'} \end{bmatrix} \begin{bmatrix} \delta p' \\ \delta_q \end{bmatrix} \tag{8}$$

In which ε_q represents deviatoric strain, the δ-sign denotes increments and K', J' and G' are stiffness parameters which can be expressed into E_v, E_h, ν_{vh} and ν_{hh}, Atkinson et al. (1990). For isotropic materials J' reaches infinity and volumetric and deviatoric stress and strain components become uncoupled.

Equation (8) can be used to find an expression for the initial pore pressure reaction. Initially the soil behaves undrained, no pore water is expelled and volumetric strain equals compression of the pore fluid. With porosity

represented by n and the bulk modulus of pore water by K_w, this yields:

$$e_0 = \frac{p'}{K'} + \frac{q}{J'} = \sigma_{w0} \frac{n}{K_w} \tag{9}$$

Inversion gives:

$$K'J'e_0 = J'(p - \sigma_{w0}) + K'q, \quad \sigma_{w0} = \frac{K_w}{n} e_0$$

$$e_0 = \left(\frac{n}{nK' + K_w} \right) \left(p + \frac{K'}{J'} q \right) = \frac{n}{K_w} \sigma_{w0} \tag{10}$$

$$\sigma_{w0} = \mathscr{B} \left(p + \frac{K'}{J'} q \right), \quad \mathscr{B} = \left(\frac{1}{\frac{nK'}{K_w} + 1} \right) \tag{11}$$

in which $\mathscr{B}$ represents the Skempton B-factor. Equation (11) is also given in Chowdhury (1978) for $\mathscr{B} = 1$. Equation (11) shows the influence of anisotropy by the ratio K'/J'. For isotropic materials $K'/J' = 0$ and the initial pore pressure increment equals the isotropic load increment. Then the isotropic effective stress remains unaltered. For $K'/J' > 0$ the initial pore pressure reaction exceeds the isotropic case, while for $K'/J' < 0$ a smaller or even negligible initial pore pressure is found. $K'/J' > 0$ is found when $E_h > E_v$ and ν_{hh} and ν_{vh} remain small. It should be noted that for a triaxial sample, loaded by an axial load increment σ_b, Eq. (11) reduces to $\sigma_w/\sigma_b = 1/3 + K'/J'$. Equation (11) equals Eqs. (6) and (7) for $t = 0$, the initial response.

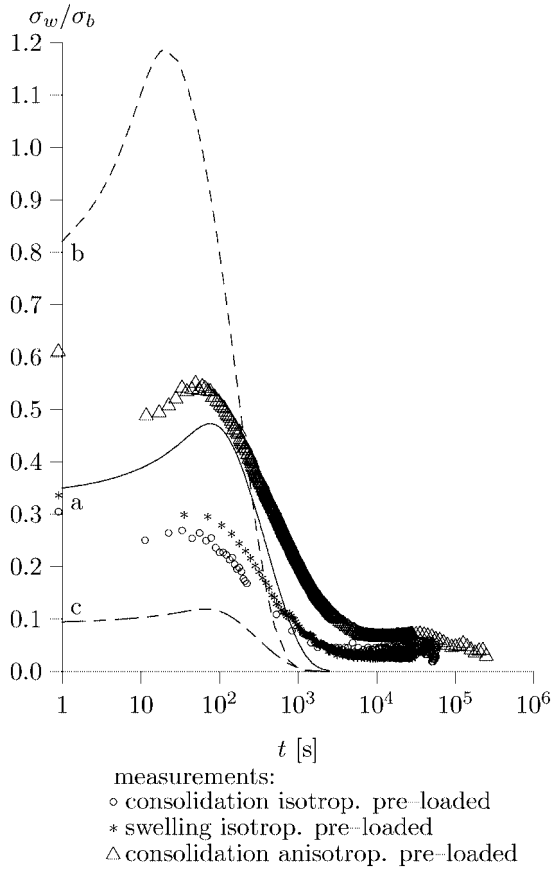

Fig. 3. Comparison between measurements and analytical solutions, *a*, *b*, *c*, according to Table 1

MEASUREMENTS

In order to validate Eqs. (6) and (7) tests are conducted. Since the Mandel-Cryer effect is found in the middle of the sample the pore pressure needs to be measured there. This is achieved by using a miniature pore pressure transducer connected to a needle. The needle is pierced through the membrane just reaching the middle. The transducer is fixed to the membrane using glue, which also prevents leakage of pore water. A stiff impermeable top cap and footing encloses the sample, providing the uniform strain conditions. Filter paper drains are placed between membrane and sample for radial drainage conditions.

In total 20 samples are tested. The samples, with diameter $d = 6.6$ cm and height $h = 8$ cm, are retrieved at Vinkeveen, near the city Utrecht, The Netherlands at a depth of approximately 1 m. After trimming the samples remaining parts are used to determine the water content $W = 5.2$ [—], loss on ignition $N = 0.57$ [—], solid density $\rho_s = 1690$ [kg/m^3]. The wet density of the tested samples was on average, after testing $\rho = 1040$ [kg/m^3].

In the first test series the samples are isotropically over-consolidated to OCR = 3. Figure 3 shows two typical measurements for this series marked by the open circle and asterix. The load increment is applied undrained, in the previous phase. The undrained loading phase is not shown in Fig. 3 except for the final value for σ_w/σ_b. It is considered to represent the initial value σ_{w0} given by Eq. (11) or by Eq. (6) at $t = 0$. Since on a logarithmic scale $t = 0$ is not given, the initial value for σ_w/σ_b is plotted at the left side of vertical axis. Equation (11) shows for isotropic material behaviour an initial value for σ_w/σ_b equal to 1/3. So Fig. 3 seems to indicate that the isotropically over-consolidated samples do not show anisotropic behaviour. Furthermore only a minor peak is found preceded by an initial decrease in pore pressure. Besides triaxial tests, oedometer and simple shear tests are conducted on horizontally and vertically retrieved samples. No significant difference in stiffness parameters is found in any of these tests. This indicates that the retrieved samples do not behave anisotropic initially, or that a possible minor anisotropy is removed when applying the isotropic pre-consolidation.

A second test series is conducted on axially pre-loaded samples. Figure 3 shows one typical measurement indicated by triangles. With σ'_{ac} the axial stress level at which the sample is pre-consolidated and the σ'_a the actual axial effective stress, the ratio σ'_{ac}/σ'_a equals 5.4. The initial value for σ_w/σ_b equals 0.6, indicating anisotropic behaviour of the tested sample. Only a minor Mandel-Cryer peak is visible.

It is remarkable that prior to the MC peak the pore pressure seems to decay such that the maximum peak value remains below the initial pore pressure reaction. Figure 3 repeats some of the analytical solutions presented by Fig. 2. Figure 3 shows a clear difference between

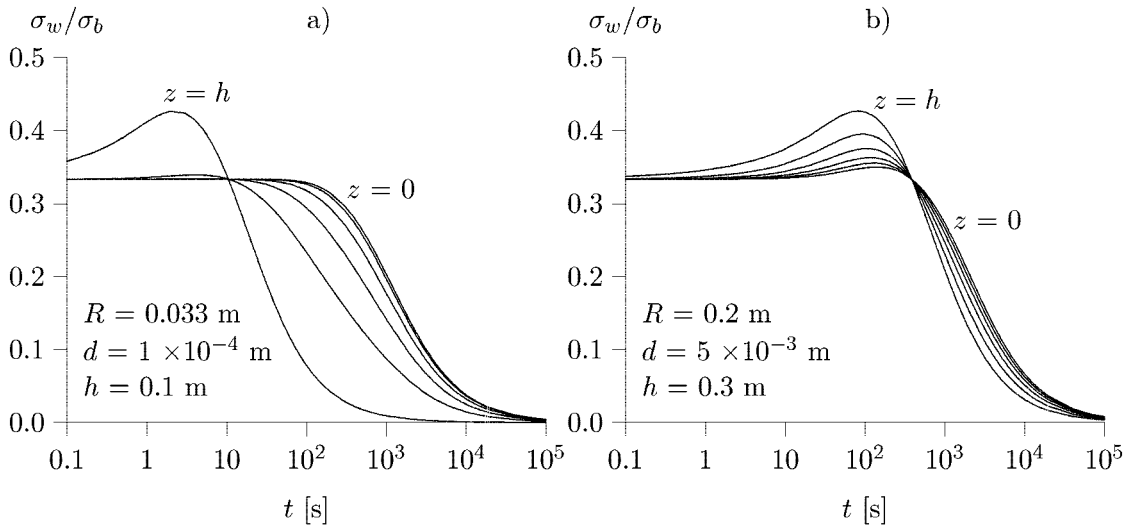

Fig. 4. Influence of drain resistance for different sample sizes, pore pressure development at $r=0$, $k=1.5\times10^{-7}$ m/s, $k'=1\times10^{-5}$ m/s

measurements and the analytical solutions. The measurements show an initial decay followed by a peak. The analytical solution presents a steeper slope after the peak then found by measurements. The analytical solution can not be fitted such that it represents correctly the initial pore pressure, the peak and the slope of the pore pressure after the peak. Three possible explanations are proposed to explain these differences between measurements and analytical solution. The first explanation is drain resistance violating the boundary condition $\sigma_w=0$ at $r=R$. The drain pressure p_d follows from:

$$\frac{d^2p_d}{dz^2}=\frac{q_0\gamma_w}{k'd}, \quad q_0=-\frac{k}{\gamma_w}\frac{\partial\sigma_w}{\partial r}$$
$$\text{with } p_d=0 \text{ at } z=h, \quad \frac{\partial p_d}{\partial z} \text{ at } z=0 \qquad (12)$$

With k' representing drain resistance and d drain thickness. Implementing the boundary condition $\sigma_w=p_d$ at $r=R$ yields a partial differential equation that can not be solved analytically. Instead an approximation method known as the Direct Method, Barends (1999), is used. Validation of this method shows that the approximation tends to underestimate the Mandel-Cryer peak and overestimates the hydrodynamic period. However the approximation clearly shows the relevant tendencies caused by influence of the drain resistance.

Figure 4 shows that the approximation for the analytical solution including drain resistance leads to sample size effects. For small samples, Fig. 4(a), the Mandel-Cryer peak is only found at the top of the sample where $p_d=0$ during the consolidation process. For larger samples Fig. 4(b), the Mandel-Cryer peak is found at each level, however the maximum value is reduced at each level. In the conventional tests the pore pressures are measured inside the specimen at just one level, i.e., the middle of the sample. So the experiments can not support nor reject the tendencies presented by Fig. 4. However, Fig. 4 shows that drain resistance is an effect that should be considered when analysing the measurement data.

A second explanation is presented by Al-Tabbaa and Wood (1991), Al-Tabbaa (1992). Here results of numerical simulation of radial consolidation for axial symmetric conditions are presented for normally consolidated samples. In absence of the uniform strain condition an initial pore pressure reduction is found which is explained by plasticity. Although, for the measurements presented in Fig. 3 the sample is enclosed by a stiff plate at the top and bottom, the pore pressure is measured in the middle of the sample at half the sample height. Probably, the uniform strain conditions does not hold at $z=h/2$ and OCR = 3 is not enough to prevent, locally, occurrence of plasticity.

The third explanation is a non-homogeneous permeability. Gibson et al. (1990) present a numerical simulation of the consolidation of a spherical sample including a variable permeability. Due to initial consolidation the permeability in the outer radius is reduced in an early stage of the consolidation process causing a retardation in the pore water flow from the inner core of the sample. This leads to a reduction in peak value and a milder slope in pore pressure development. These observations correspond to the measurements presented in Fig. 3.

LARGE SCALE TESTING

To test the scale effects shown by Fig. 4 a large scale triaxial test is conducted. The sample dimensions are presented by Table 2. A stiff plate is placed at the top and bottom of the sample. The pore pressure transducer is connected to the stiff plate at the top of the sample protruding into the peat by approximately 3 cm.

The sample is retrieved from a peat embankment in Wilnis, The Netherlands, Bezuijen et al. (2005). After finishing the test, the water content $W=0.544$ [—] density $\rho=1.51$ t/m^3 and loss on ignition $N=0.80$ [—] are derived.

Figure 5 shows the applied loading path. After consoli-

Table 2. Initial and final sample dimensions

Parameter	Initial value	Final value
Diameter [m]	0.42 ± 0.005	0.42 ± 0.005
Height [m]	0.61 ± 0.005	0.50 ± 0.005
Weight [kg]	77.5 ± 0.05	67.4 ± 0.05
Density [kg/m^3]	940 ± 4	960 ± 6

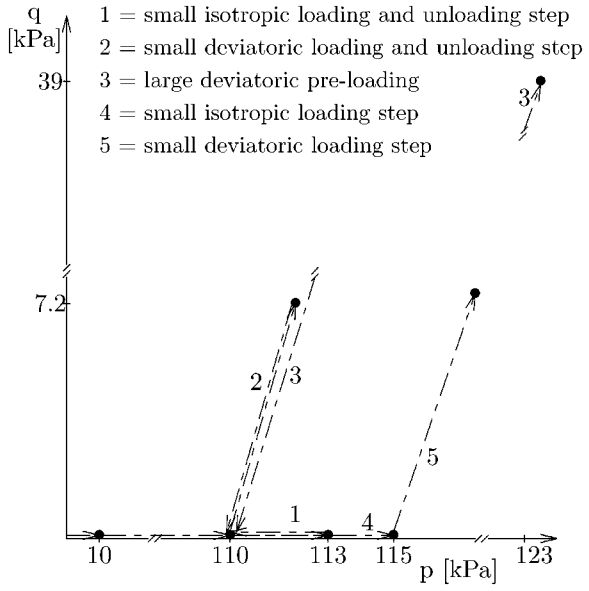

Fig. 5. Applied loading path

dation at 10 kPa a back-pressure of 100 kPa is used. In step 1, the sample is consolidated at an isotropic cell pressure of 113 kPa followed by reduction in cell pressure is reduced to 110 kPa followed by a swelling phase. In step 2 an undrained axial load is applied, followed by a consolidation phase. The pore pressure development found in this consolidation phase is presented by Fig. 6. Next the sample is unloaded by removing the axial load undrained followed by a swelling phase. Figure 6 presents the pore pressure development found in this phase. In step 3 the same sample is consolidated under a deviatoric pre-load. With σ'_v the actual vertical effective stress and σ'_{vc} the maximum effective vertical stress, the level of axial pre-loading is presented by $\sigma'_v/\sigma'_{vc}=5.4$, followed by an unloading and swelling phase. A small isotropic load increment is applied in step 4, followed by a small axial load increment, step 5. This increment is applied undrained followed by a consolidation phase, which is shown by Fig. 6.

Figure 7 shows the results for curve fitting Eqs. (6) and (7) to the measurement data from steps 4 and 5. The fitted stiffness parameters are presented next to the graph. The actual value for E_v is found from the deviatoric pre-consolidation phase, by the initial tangent line of the $q-\varepsilon_a$ curve. Next by trial and error, values are found for E_h, ν_{hh} and ν_{vh} which represent the initial excess pore pressure and the peak value. Finally, a value for the permeability needs to be found such that the time of occurrence of the peak as well as the slope of the pore pressure development correspond to the measurements.

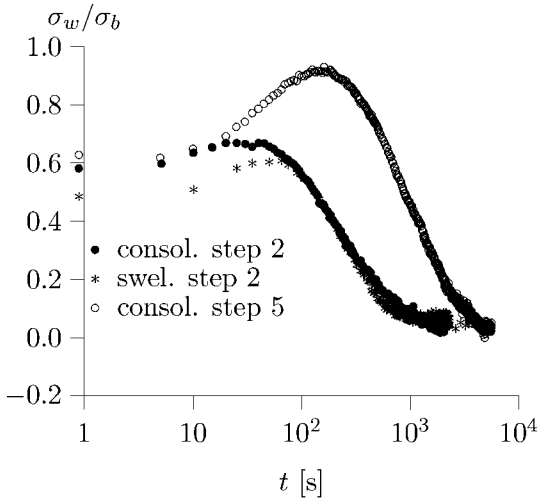

Fig. 6. Pore pressure development at $r=0$ after an axial load increment

From the test results the permeability could not be found independently from the stiffness parameters since all steps consist of either undrained loading or consolidation. The test set-up did not allow for a classical constant head or falling head test. Instead a number of constant rate of strain oedometer tests, CRS tests, are conducted on samples retrieved in the vicinity of the location where the large sample has been retrieved. The measurements are used to fit Eq. (13), in which k_0 represents the permeability at e_0 and χ is a coefficient to be derived from measurements;

$$k = k_0 \exp(-\chi e) \tag{13}$$

In total 10 samples have been tested. On average $\chi=8.5$ is found indicating a strongly varying permeability and $k_0=4.5\times10^{-8}$ m/s. These measurements were used in the analysis of the large scale test. For a proper reproduction of the time of occurrence of the peak and the slope of pore pressure development some adjustment of k-value is needed. Equations (6) and (7) include a constant k-value. Therefore, Fig. (7) presents a different, actual, value for each loading step. This value is assumed to be constant during the loading step for which it is derived. The adjustment can be fully explained by the heterogeneity of peat. It should be noted that large peat samples will include a larger heterogeneity scale which, in general, lead to a larger permeability for larger samples.

For step 2 however no accurate fit can be found. Again the analytical solution will overestimate the peak and predict a steeper slope. The previous section discusses three optional causes for the differences between analytical solution and measurements. Firstly, to check the validity of boundary condition, $\sigma_w=0$ at $r=R$, the drain pressure is measured in the tube connecting the porous stone to the pore water collection device. Measurements indicate that the drain resistance is negligible. All cases clearly show the Mandel-Cryer effect. Secondly, the initial decrease in pore pressure found in the small sample triaxial tests is absent.

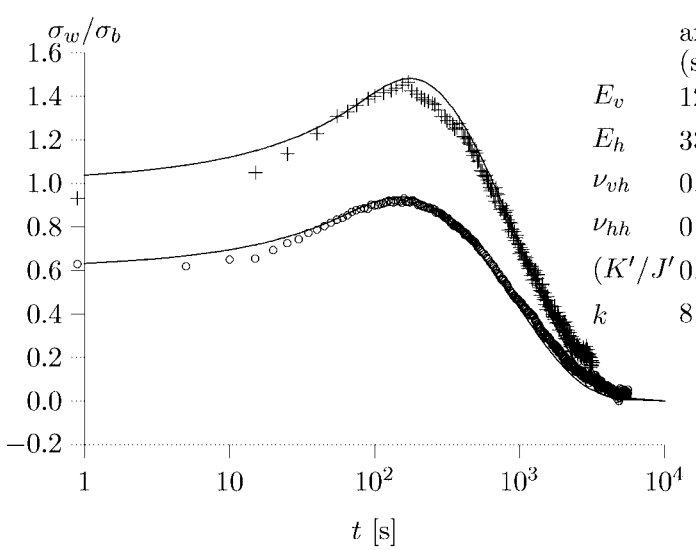

	○ axial load incr. (step 5)	+ isotropic load incr. (step 4)
E_v	1200 kPa	1200 kPa
E_h	3300 kPa	3300 kPa
ν_{vh}	0.1	0.1
ν_{hh}	0	0.1
$(K'/J'$	0.27	0.3)
k	8×10^{-8} m/s	6×10^{-8} m/s

Fig. 7. Analytical fit for measurement data step 4 and 5

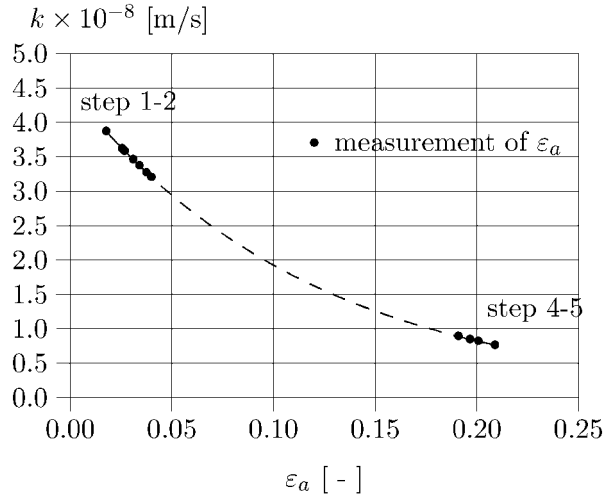

Fig. 8. Illustration of decay in permeability during the test, based on axial strain

Thirdly, as mentioned earlier, a non-homogeneous permeability is found in the CRS tests on conventional sized samples retrieved from the direct surroundings of the large-scale sample. To get an impression on the development of the permeability during the test Eq. (13) is applied in combination to the deformation measurements during the test. Due to malfunction of the triaxial device in the early stages of the test a continuous measurement of expelled pore water volume is not available. However since radial deformations remain small the vertical strain gives a reasonable indication for volumetric strain. Using Eq. (13), Fig. 8 illustrates the development in k during the test for $k_0 = 4.5 \times 10^{-8}$ m/s and $\chi = 8.5$. It should be noted that the value for k presented in Fig. 7 exceeds the value for k_0 found for the CRS tests.

Figure 8 shows that the permeability decays during the steps 1–3 indicating a strong influence for these steps. After the deviatoric pre-consolidation the permeability is strongly reduced which invokes retardation of the consolidation process. This is in agreement to Figs. 6 and 7.

CONCLUSIONS

Anisotropy in stiffness strongly influences the pore pressure development during consolidation of a triaxial sample. This is mainly found by the initial pore pressure reaction and the size of the Mandel-Cryer effect.

The conventional sized samples show only a negligible Mandel-Cryer effect. A large scale sample shows clearly the Mandel-Cryer effect for axially pre-consolidated conditions. The analytical solution can perfectly be fitted to the measurements on the large scale tests.

Three possible explanations are proposed by literature why measurements on conventional triaxial samples for peat do not correspond to the analytical solution. These are drain resistance, non uniform axial deformation and varying permeability. The first two might be solved by a proper test set-up. However the variability in permeability depends on the tested material and load history. So, for peat, measurements of the Mandel-Cryer effect is not appropriate for the assessment of anisotropic stiffness parameters.

REFERENCES

1) Abousleiman, Y., Cheng, A. H. D., Cui, L., Detournay, E. and Roegiers J.-C. (1996): Mandel's problem revisited, *Géotechnique*, **46** (2), 187–195.
2) Al-Tabbaa, A. and Wood, D. M. (1991): Horizontal drainage during consolidation: insights gained from analyses of a simple problem, *Géotechnique*, **41** (4), 571–585.
3) Al-Tabbaa, A. (1992): Finite element analyses of consolidation with radial peripheral drainage. *Num. Models in Geomech.*, (eds. by Pande and Pietruszczak), 4th Int. Sym. on Num. Models in Geomech., Swansea.
4) Atkinson, J. H., Richardson, D. and Stallebrass, S. E. (1990): Effect of recent stress history on the stiffness of overconsolidated

soil, *Géotechnique*, **40** (4), 531–540.
5) Barends, F. B. J. (1999): IDM for transient problems, *Geotechnical Engineering for Transportation Infrastructure*, (eds. by Barends et al.), Balkema, Rotterdam ISBN 90-5809-047-7.
6) Bezuijen, A., Kruse, G. A. M. and Van, M. A. (2005): Failure in peat dikes, *Proc. 16th ICSMGE*, Osaka, Rotterdam, Millpress, **3**, 1857–1860.
7) Biot, M. A. (1941): General theory of three dimensional consolidation, *J. Applied Physics*, **12**, 155–164.
8) Biot, M. A. (1955): Theory of elasticity and consolidation for a porous anisotropic solid, *J. Applied Physics*, **26**, 182–185.
9) Biot, M. A. and Willis, D. G. (1957): The elastic coefficients of the theory of consolidation, *J. Applied Mechanics*, **24**, 594–601.
10) Brodeau, A. (1946): Corps anisotropes symtries naturelles, *Publications Scientifiques et Techniques du ministre de l'air*, (201) (in French).
11) Chen, S. L., Zhang, L. M. and Chen, L. Z. (2005): Consolidation of a finite transversely isotropic soil layer on a rough impervious base, *J. Engrg. Mech.*, **121** (2), 1279–1290.
12) Chowdhury, R. N. (1978): Effective stress parameters of anisotropic soil, *J. Geotech. Engrg. Div.*, (GTI), 124–128.
13) Cryer, C. W. (1963): A comparison of the three dimensional consolidation theories of Biot and Terzaghi, *Quart. J. Mech. Applied Mathematics*, **XVI**, 401–412.
14) De Leeuw, H. E. (1964): Consolidatie in drie dimensies, VII cilindervormige symmetrie, *LGM mededelingen*, (2), 17–48 (in Dutch).
15) De Leeuw, H. E. (1965): The theory of three-dimensional consolidation applied to cylindrical bodies, *Proc. 6th ICSMFE*, *sect* 2/23 Montreal 287.
16) Gibson, R. E., Knight, K., Taylor, P. W. (1964): A critical experiment to examine theories of three dimensional consolidation, *Eur. Conf. Soil Mech.*, Wiesbaden, 1–17.
17) Gibson, R. E., Gobert, A. and Schiffmann, R. L. (1990): On Cryer's problem with large displacements and variable permeability, *Géotechnique*, **40** (4), 627–631.
18) Kumamoto and Yoshikuni (1981): A key to solution of the irrotational consolidation and its application to cylindrical clay, *Soils and Foundations*, **21** (2), 35–46.
19) Mandel, J. (1953): Consolidation des sols (étude mathématique), *Géotechnique*, **3** 287–299 (in French).
20) Verruijt, A. (1969): Elastic storage of aquifers, *Flow through Porous Media*, (ed. by de Wiest), R. J. M. Academic Press.
21) Zwanenburg, C. (2005): The influence of anisotropy on the consolidation behaviour of peat, *PhD Thesis*, TUDelft, ISBN 90-407-2615-9 Delft University Press.

APPENDIX: ANALYTICAL SOLUTION OF THE PORE PRESSURE DEVELOPMENT

SOLUTION discusses the analytical solution to the cross-anisotropic consolidation problem given by Eq. (5). This appendix discusses the derivation of the analytical solution Eqs. (6) and (7). The following symbols are used:

A, B, D, $2G_{hh}$ = Stiffness parameters defined in Eq. (2)
C_1, C_2, C_3, C_4 = Integrational constants to be solved by boundary conditions
J_0, J_1, Y_0, Y_1 = Bessel functions
e, e_0 = volumetric strain, initial volumetric strain
K', J' = Stiffness parameters defined by Eq. (8)
k = permeability
t = time
r, θ, z = co-ordinates of axial symmetry
R = radius of sample, *see* Fig. 1
s = parameter in Laplace transform
u_r, u_z = displacement in radial, respectively in vertical direction as defined by Fig. 1
γ_w = volumetric weight of water
σ_r, σ_θ, σ_z = total stress in r, θ and z direction
σ'_r, σ'_θ, σ'_z = effective stress in r, θ and z direction
σ_b = load applied at the top, *see* Fig. 1

The consolidation problem is given by Eq. (5):

$$\nabla^2 e = \frac{1}{c}\frac{\partial e}{\partial t}, \quad c = k[A + 2G_{hh}]/\gamma_w \tag{14}$$

Equation (14) can be solved by the Laplace transformation. With the overbar denoting the Laplace transform, the following is found:

$$\nabla^2 \bar{e} = \frac{1}{c}[s\bar{e} - e_0], \quad e_0 = 0$$

$$\nabla^2 \bar{e} = \frac{s}{c}\bar{e}, \quad \rightarrow \quad \frac{\partial^2 \bar{e}}{\partial r^2} + \frac{1}{r}\frac{\partial \bar{e}}{\partial r} - \frac{s}{c}\bar{e} = 0 \tag{15}$$

Equation (15) is solved by a standard solution:

$$\bar{e} = C_1 J_0(\lambda r) + C_2 Y_0(\lambda r), \quad \lambda = \sqrt{\frac{-s}{c}} \tag{16}$$

Application of the Laplace transform to Eq. (3) yields:

$$[A + 2G_{hh}]\nabla^2 \bar{e} = \nabla^2 \bar{\sigma}_w, \quad \nabla^2 \bar{e} = \frac{\nabla^2 \bar{\sigma}_w}{A + 2G_{hh}}$$

$$\bar{e} = \frac{1}{A + 2G_{hh}}\bar{\sigma}_w + C_3, \quad \nabla^2 C_3 = 0 \tag{17}$$

Combination of Eq. (16) to Eq. (17) yields:

$$\bar{\sigma}_w = [A + 2G_{hh}][C_1 J_0(\lambda r) + C_2 Y_0(\lambda r) - C_3] \tag{18}$$

The volumetric strain is defined by:

$$\bar{e} = \frac{1}{r}\frac{\partial(r\bar{u}_r)}{\partial r} + \frac{\partial \bar{u}_z}{\partial z} \tag{19}$$

which yields with Eq. (16):

$$\frac{1}{r}\frac{\partial(r\bar{u}_r)}{\partial r} = C_1 J_0(\lambda r) + C_2 Y_0(\lambda r) - \frac{\partial \bar{u}_z}{\partial z}$$

Integration of Eq. (19) gives:

$$\frac{\bar{u}_r}{R} = C_1 \frac{J_1(\lambda r)}{\lambda R} + C_2 \frac{Y_1(\lambda r)}{\lambda R} - \frac{r}{2R}\frac{\partial \bar{u}_z}{\partial z} + \frac{C_4}{rR} \tag{20}$$

Differentiation of Eq. (19) results in:

$$\frac{\partial \bar{u}_r}{\partial r} = C_1\left[J_0(\lambda r) - \frac{J_1(\lambda r)}{\lambda r}\right] + C_2\left[Y_0(\lambda r) - \frac{Y_1(\lambda r)}{\lambda r}\right] - \frac{1}{2}\frac{\partial \bar{u}_z}{\partial z} - \frac{C_4}{r^2} \tag{21}$$

Using Eq. (2) stress and strain can be expressed by:

$$\bar{e} = C_1 J_0(\lambda r) + C_2 Y_0(\lambda r) \tag{22}$$

$$\bar{\sigma}_w = [A + 2G_{hh}][C_1 J_0(\lambda r) + C_2 Y_0(\lambda r) - C_3] \tag{23}$$

$$\bar{\sigma}_r' = A[C_1 J_0(\lambda r) + C_2 Y_0(\lambda r)] + 2G_{hh}\left[\begin{array}{l} C_1\left[J_0(\lambda r) - \dfrac{J_1(\lambda r)}{\lambda r}\right] \\ + C_2\left[Y_0(\lambda r) - \dfrac{Y_1(\lambda r)}{\lambda r}\right] - \dfrac{1}{2}\dfrac{\partial \bar{u}_z}{\partial z} - \dfrac{C_4}{r^2}\end{array}\right] + B\frac{\partial \bar{u}_z}{\partial z} \tag{24}$$

$$\bar{\sigma}_\theta' = A[C_1 J_0(\lambda r) + C_2 Y_0(\lambda r)] + 2G_{hh}\left[C_1\frac{J_1(\lambda r)}{\lambda r} + C_2\frac{Y_1(\lambda r)}{\lambda r}\right] + 2G_{hh}\left[\frac{C_4}{r^2} - \frac{1}{2}\frac{\partial \bar{u}_z}{\partial z}\right] + B\frac{\partial \bar{u}_z}{\partial z} \tag{25}$$

$$\bar{\sigma}_\theta' = (A + B)[C_1 J_0(\lambda r) + C_2 Y_0(\lambda r)] + D\frac{\partial \bar{u}_z}{\partial z} \tag{26}$$

$$\bar{\sigma}_r = \bar{\sigma}_r' + \bar{\sigma}_w, \quad \bar{\sigma}_\theta = \bar{\sigma}_\theta' + \bar{\sigma}_w, \quad \bar{\sigma}_z = \bar{\sigma}_z' + \bar{\sigma}_w \tag{27}$$

Since $\bar{e}$ and $\bar{\sigma}_r$ have a finite value at $r = 0$ it is found that $C_2 = C_4 = 0$. Three unknown parameters, C_1, C_3 and $\partial \bar{u}_z / \partial z$ are to be solved by boundary conditions. In general the boundary conditions are given by:

a) at $r = R$ $\sigma_w = g_1$, $\rightarrow$ $\bar{\sigma}_w = \bar{g}_1$

b) at $r = R$ $\sigma_r = g_2$, $\rightarrow$ $\bar{\sigma}_r = \bar{g}_2$

c) at $z = h$ $1/A \int 2\pi r \sigma_z \, dr = g_3$, $\rightarrow$ $1/A \int 2\pi r \bar{\sigma}_z \, dr = \bar{g}_3$

From boundary condition a and Eq. (23) the following is found:

$$C_3 = C_1 J_0(\lambda R) - \frac{\bar{g}_1}{A + 2G_{hh}} \tag{28}$$

Equations (27), (24), (23), (28) and boundary condition b yield:

$$\frac{\partial \bar{u}_z}{\partial z} = \frac{C_1}{B - G_{hh}}\left[(A + 2G_{hh}) J_0(\lambda R) - 2G_{hh}\frac{J_1(\lambda R)}{\lambda R}\right] + \frac{\bar{g}_1 + \bar{g}_2}{B - G_{hh}} \tag{29}$$

Equations (27), (26), (23), (28), (29) and boundary condition c yield:

$$C_1 = \frac{\dfrac{D(\bar{g}_1 + \bar{g}_2)}{B - G_{hh}} - \bar{g}_3 - \bar{g}_1}{2\dfrac{J_1(\lambda R)}{\lambda R}\left[B - 2G_{hh} + \dfrac{DG_{hh}}{B - G_{hh}}\right] + (A + 2G_{hh}) J_0(\lambda R)\left[1 - \dfrac{D}{B - G_{hh}}\right]} \tag{30}$$

Axial Loading

The solution for the pore pressure development the axially loaded sample is elaborated. The corresponding boundary conditions are presented by $\bar{g}_1 = \bar{g}_2 = 0$, $\bar{g}_3 = \bar{\sigma}_b$. Equation (23) is then given by:

$$\frac{\bar{\sigma}_w}{\sigma_b} = \frac{J_0(\lambda R) - J_0(\lambda r)}{s\left[\dfrac{2J_1(\lambda R)}{[A + 2G_{hh}]\lambda R}\left[(B - 2G_{hh}) + \dfrac{DG_{hh}}{B - G_{hh}}\right] + J_0(\lambda R)\left(1 - \dfrac{D}{B - G_{hh}}\right)\right]} \tag{31}$$

The Heaviside expansion theorem is used to find the inverse transform of Eq. (31). A removable root is found for $s = 0$, the other roots satisfy the following equation:

$$\frac{J_1(\lambda R)}{J_0(\lambda R)} = \frac{1}{2}\left[\frac{A + 2G_{hh}}{B - 2G_{hh} + \dfrac{DG_{hh}}{B - G_{hh}}}\right]\left[\frac{D}{B - G_{hh}} - 1\right]\lambda R \tag{32}$$

The values for s that fulfil Eq. (32) are indicated by s_j. The expression for σ_w is now given by:

$$\frac{\sigma_w}{\sigma_b} = \sum_{j=1}^{\infty} \frac{\left[1 - \dfrac{J_0(\lambda_j r)}{J_0(\lambda_j R)}\right]\exp(s_j t)}{\left[\dfrac{B - 2G_{hh} + DG_{hh}/(B - G_{hh})}{A + 2G_{hh}}\right] + \left[\dfrac{\lambda_j R}{2}\dfrac{J_1(\lambda_j R)}{J_0(\lambda_j R)} - 1\right]\left[\dfrac{D}{B - G_{hh}} - 1\right]} \tag{33}$$

Isotropical Loading

Using Eqs. (18), (28) and (30) the pore pressure development for isotropic loading is found. For the corresponding boundary conditions $g_1 = 0$ and $g_2 = g_3 = \sigma_b$ it follows that:

$$\frac{\bar{\sigma}_w}{\sigma_b} = \frac{J_0(\lambda R) - \dfrac{B - G_{hh} - D}{B - G_{hh}} J_0(\lambda r)}{s\left[\dfrac{2 J_1(\lambda R)}{[A + 2G_{hh}]\lambda R} \left[(B - 2G_{hh}) + \dfrac{D G_{hh}}{B - G_{hh}} \right] + J_0(\lambda R) \left(1 - \dfrac{D}{B - G_{hh}} \right) \right]} \tag{34}$$

The inverse transform gives:

$$\frac{\sigma_w}{\sigma_b} = \sum_{j=1}^{\infty} \frac{\dfrac{B - G_{hh} - D}{B - G_{hh}} \left[1 - \dfrac{J_0(\lambda_j r)}{J_0(\lambda_j R)} \right] \exp(s_j t)}{\left[\dfrac{B - 2G_{hh} + D G_{hh}/(B - G_{hh})}{A + 2G_{hh}} \right] + \left[\dfrac{\lambda_j R}{2} \dfrac{J_1(\lambda_j R)}{J_0(\lambda_j R)} - 1 \right] \left[\dfrac{D}{B - G_{hh}} - 1 \right]} \tag{35}$$

Note that the reciprocal value for the constant $(B - G_{hh} - D)/(B - G_{hh})$ can be rewritten, using Eq. (2):

$$\frac{B - G_{hh}}{B - G_{hh} - D} = -\left(\frac{1}{3} + \frac{K'}{J'} \right)$$